Analytical Methods

Accepted Manuscript

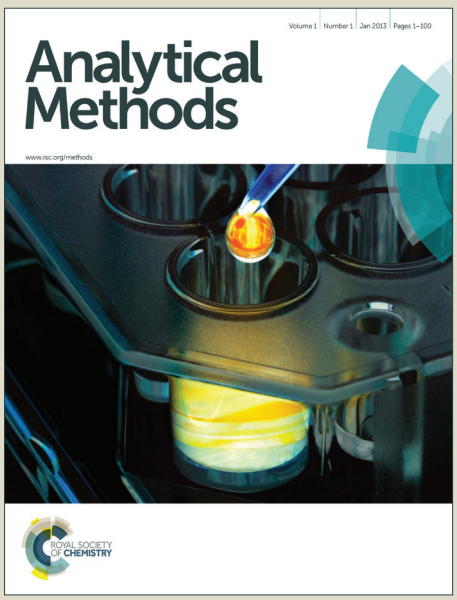

ROYAL SOCIETY OF CHEMISTRY

www.rsc.org/methods

Graphical abstract

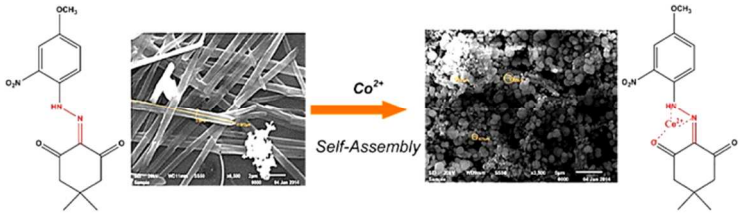

A new highly selective β-diketones of aryl hydrazone chemosensor for Co^{2+} have been designed and exhibits excellent sensing ability under neutral pH.

Facile, cost effective synthesis and DFT based studies of substituted aryl hydrazones of β-diketones: A new selective Fluorescent Chemosensor for Co^{2+}

Annamalai Subhasri and Chinnadurai Anbuselvan*

Department of Chemistry, Annamalai University, Annamalainagar − 608 002, India

Corresponding author email: cas_amu@yahoo.co.in

*Corresponding author: Address

C. Anbuselvan

Assistant professor,

Department of Chemistry

Annamalai University

Annamalainagar 608 002

E-mail: *cas_amu@yahoo.co.in*

An intramolecular charge transfer (ICT) chromophore 2-(2-(4-methoxy-2-nitrophenyl)hydrazono)-5,5-dimethylcyclohexane-1,3-dione (CD1), 2-(2-(4-methyl-2-nitrophenyl)hydrazono)-5,5-dimethylcyclohexane-1,3-dione (CD2) have been synthesized and firstly used as a chemosensor with a reversible "on-off" sensing capability for biologically and environmentally significant Co^{2+} with a detection limit of 3 μm to 7 μm. The new metal ion sensors that contain hydrazones of β-diketones have been synthesized and characterized FT-IR, ^{1}H, ^{13}C NMR spectra, Scanning electron microscopy (SEM) and Single crystal X-ray diffraction studies. The FT-IR and NMR spectral data clearly show the effective intramolecular hydrogen bonding in all synthesized substituted hydrazones. SEM was employed to investigate their morphology. A single crystal X-ray diffraction study confirms the exact structure of the CD1 and CD2. Packing diagram explains the strong intramolecular hydrogen bonding in CD1 and CD2 molecule. The absorption spectrum is all similar respective of substituent and solvent. By comparison the fluorescence is strongly dependent on the electronic character of the substituent. The sensors show excellent selectivity and sensitivity with fluorescence enhancement to Co^{2+} over other cations in ethanol aqueous solution. A combined experimental and theoretical studies were conducted on the molecular structure using density functional methods (B3LYP) invoking 6-31G basis set. The optimized geometric bond lengths and bond angles obtained by the DFT method shows good agreement with the experimental values. The energy of the highest occupied molecular (HOMO) orbital and lowest unoccupied (LUMO) molecular orbital has been predicted

Introduction

Development of fluorescent devices for the sensing of chemical species are currently of significant for chemistry, biology, and environmental science. The fluorescent sensors for selective and sensitive detection of metal ions increased more attention nowadays. So far, the development of practical fluorescent chemosensors for many heavy and transition metal ions is still a challenge such as the Zn(II)[1,2], Ag(I)[3], Fe(III)[4] and Cu (II)[5] ions.

Cobalt is a naturally occurring element in rocks, soils, water, animals, and plants. However, exposure to extreme amounts of cobalt in the environment may result in various adverse health effects such as mutagenesis, cardiotoxicity, asthma, lung fibrosis, and even lung cancer. It is well known that Co^{2+} as one of the most important transition metal ion plays an important role in the metabolism of iron and synthesis of hemoglobin, and it is also a main component of Vitamin B12 and other biological compounds[6]. Cobalt deficiency in the human body may lead to a pathological condition and it is also a significant environmental pollution[7]. Consequently, there has been a growing interest in the development of selective Co^{2+} sensor for biological and environmental applications. However, there are only a few sensors based on fluorescence reported for cobalt ion determination. Most of the fluorophores respond to cobalt ion only in the presence of oxidizing agents only[8]. Moreover, some of fluorophores posses poor selectivity[9] and relatively high back ground[10]. Therefore, searching for new fluorophores for the determined cobalt ions with excellent analytical performance characteristic is still a challenge. Because of the fluorescence quenching nature of paramagnetic Co(II), fluorescence-enhanced probes for cobalt are very scarce.

Aryl hydrazones are important classes of compounds which have long attracted attention, owing to their remarkable biological and pharmacological properties, such as antibacterial, antiviral, antineoplastic, and antimalarial activities.[11] The hydrazone derivatives, functional diversity of this azomethine group, which is characterized by the triatomic structure C=N–N, that enables its use in numerous fields, it has (i) nucleophilic imine and amino-type (more reactive) nitrogens, (ii) an imine carbon that has both electrophilic and nucleophilic character, (iii) configurational isomerism restricting from the intrinsic environment of the C=N double bond, and (iv) in most cases an acidic N–H proton. These structural subjects give the hydrazone group its physical and chemical properties, in addition to playing a vital part in determining the range of applications it can be involved in. A number of factors that decide the hydrazone functional group from its imine counterpart, namely: (i) the stability of the C=N double bond to hydrolysis under neutral conditions because of a mesomeric effect; (ii) the existence of an extra amino-type nitrogen in the system that enhances this group's coordination capability; and (iii) the acidic N–H proton that can be utilized in intramolecular H-bonding, anion sensing and even coordination with metals. Hydrazines, hydrazides and hydrazones are central precursors for the synthesis of heterocycles, pharmaceuticals, Agrochemicals, polymers, dyestuffs and photography products[12].

The resonance-assisted hydrogen bond systems involve a synergistic reinforcement of hydrogen bonds by the delocalization of a π-conjugated chain connecting donor and acceptor atoms; they have been applied for the activation of a carbon in a position to a carbonyl, induced enolization in keto-enol tautomerism, controlled crystal packing, formation of bistable H-bonds in functional molecular materials, activation of dinitriles towards formation of amidines, carboxamides and iminoesters, etc. while special interest should be paid to the nature of the strong intramolecular O…H−N resonance-assisted hydrogen bond and its influence on the enol-

azo ⇌ hydrazone transformation.[13-16] The rich tautomerism and isomerism of aryl hydrazones together with the intramolecular resonance assisted hydrogen bond system can be applied for regulation of tautomerization-isomerization, activation of the carbon in α position to a carbonyl, antiferroelectric paraelectric transition, regioselective activation of dinitriles, catalysis, ligand liberation, etc.[17] In some cases hydrogen bonding acts as an active site for initiation of chemical reaction. However, the studies are very few in the literature and in view of the significance of arylhydrazone derivatives in medicinal and structural chemistry it was thought worthwhile to synthesize some arylhydrazone derivatives of diketones like dimedone.[18] These results led to the observation that the system exists in a conformation with a preferred orientation where the stereoelectronic constraints and the stabilizing effect of hydrogen bonding are competing.

The absorption spectra of hydrazones are generally bathochromatically shifted with respect to corresponding azo tautomers; the effect of polar substituents on absorption maxima is mutually opposite.[19, 20] Hydrazone tautomers quite often fluoresce, example for the derivatives of pyrazolone hydrazones.[21] Only hydrazone fluorescence was observed in the case, where both tautomers were present, and thus excited state intramolecular proton transfer process (from oxygen to nitrogen) was detected by comparison of absorption and fluorescence excitation spectra.[22,23] The novel ratiometric probe CD1 and CD2 developed herein represents the good example of a hydrazone-dione ratiometric fluorescent cobalt probe with several highly favorable features, in particular, a remarkable ratiometric fluorescence response for effective applications in environmental settings. This signaling mechanism for ion-responsive probes to generate a large ratiometric fluorescence response should lead to the development of powerful fluorescence probes with large emission intensity ratios for useful applications in many fields[24].

In the present work, a series of substituted aryl hydrazones of β-diketone were synthesized and characterized by FT-IR, UV, NMR and confirmed by Single crystal X-ray diffraction studies. This sensor fluorescence in the presence of metal ions in polar organic solvents.The fluorescence response in polar organic solvents is selective for Co^{2+} and the binding is strong. Another one objective of this paper is to find theoretical methods that would offer a higher certainty of finding molecular structure parameters. In addition to this HOMO, LUMO, NBO analysis has been used to reveal the information regarding charge transfer within the molecule.

Experimental

All the solvents and reagents were analytical reagent grade . The homogeneity of the compounds was monitored by ascending thin layer chromatography (TLC) on silica gel-G (Merck) coated aluminum plates, visualized by iodine vapor and UV light. Compounds were prepared by the general procedure (Scheme 1) which anilines (0.5 mmol) were dissolved separately in 1 N HCl (25 cm^3) at 0-5°C temperature and in each case cooled aqueous solution (10 cm^3) of $NaNO_2$ (0.40 g) was added drop wise with stirring followed by the addition of dimedone (0.70 g, 0.5 mmol) and sodium acetate (5.0 g) dissolved in water (30 cm^3). Corresponding mixtures were further stirred for 4 h at room temperature (25 °C). Solids thus obtained were filtered and washed several times with water, followed by ethanol and then dried in a vacuum. The crude products were crystallized in ethanol. Compounds CD1 and CD2 were purified by column chromatography by using benzene as eluent. Yield and melting points of the derived compounds are mentioned below.

IR spectra were recorded on an Avatar Nicholet FT-IR spectrophotometer (range 4000–400 cm^{-1}) in KBr pellets (λ_{max} in cm^{-1}). ^1H and ^{13}C NMR spectra for analytical purpose were

recorded in $CDCl_3$ on a Bruker instrument at 400 MHz, chemical shifts are expressed in d-scale downfield from TMS as an internal standard. SEM analysis was performed for surface morphology of CD1, CD2 and complexes, on gold coated samples using a JEOL JSM-5610 SEM. UV–vis spectra were recorded on a SHIMADZU UV-1650PC digital spectrophotometer by dissolving the sample in spectral grade ethanol using a 1 cm path length quartz cell. A Perkin Elmer LS 55 fluorescence spectrometer was employed to record the fluoresence (FL) spectra at room temperature. The choice of excitation wavelengths was based on the absorbance spectral characteristics.

Estimation of Metal salts

A stock solution of compound CD1 (3.0×10^{-3}) and CD2 (1.0×10^{-3} M) were prepared in CH_3CH_2OH/H_2O (4:1, v/ v). Solutions of 2.0×10^{-4} M salts of the respective cation were prepared in distilled water. All experiments were carried out in CH_3CH_2OH/H_2O solution (CH_3CH_2OH/H_2O = 4:1, v/v, 10 μM HEPES buffer, pH = 7.0). In titration experiments, each time at 4×10^{-5} M solution of CD1 and CD2 were filled with a quartz optical cell of 1 cm optical path length, and the ion stock solutions were added into the quartz optical cell gradually by using a micropipet. Spectral data were recorded at 1 min after the addition of the ions. In selectivity experiments, the test samples were prepared by placing appropriate amounts of the anions/ cations stock into 2 mL of solution of CD1 (3.0×10^{-3}) and CD2 (1.0×10^{-3} M)[25].

X-ray structure determinations

The X-ray quality single crystals of CD1 and CD2 were immersed in cryo-oil, on a glass fiber and transferred to the cold gas stream of the diffractometer (Bruker SMART APEX). Measurements were performed to 2θ max 52° with monochromated Mo Kα radiations of 24102 measured reflections, 4563 were unique (R_{int} = 0.026) and were used for all calculations.

Structure refinement: The structures were refined anisotropically against F2 (programme SHELXL-97). Calculations were performed using the WINGX System-Version 1.80.03. All hydrogen atoms were inserted in calculated positions. Least square refinements with anisotropic thermal motion parameters for all the non-hydrogen atoms and isotropic for the remaining atoms were employed.

Computational details

The entire calculations were performed at ab initio DFT levels using Gaussian 03W[26] program package, invoking gradient geometry optimization[27]. Initial geometry generated from standard geometrical parameters was minimized without any constraint in the potential energy surface at ab initio adopting the standard 6- 31G basis set.

Results and discussion

2-(2-(4-methoxy-2-nitrophenyl)hydrazono)-5,5-dimethylcyclohexane-1,3-dione (CD**1)**

Yellow solid, yield: 98%, m. p. 182 °C; IR (KBr,cm^{-1}) 3466, 3107, 3012, 2974, 2953, 1703, 1739, 1639 (**Fig. S1**); 1H NMR (400 MHz, $CDCl_3$) (δ): 1.08 (s, CH_3), 2.59 and 2.62 (s, CH_2), 3.84 (s, OCH_3), 7.25 - 8.24 (aromatic protons), 16.01 (s, NH) (**Fig. S3)**; 13C NMR (125 MHz, $CDCl_3$) (δ) 28.6, 30.6, 52.7, 52.9, 56.2, 108.3, 120.3, 124.1, 131.7, 132.2, 136.8, 157.2, 193.6, 196.4 (**Fig. S4**).

2-(2-(4-methyl-2-nitrophenyl)hydrazono)-5,5-dimethylcyclohexane-1,3-dione (CD**2)**

Yellow solid, yield: 90%, m. p 178 °C; IR (KBr, cm^{-1}) 3421, 2948, 2924, 2869, 1685, 1642, 1568 (**Fig. S2**); 1H NMR (400 MHz, $CDCl_3$) (δ): 1.08 (s, CH_3), 2.59 and 2.62 (s, CH_2),

3.84 (s, OCH_3), 7.25-8.24 (aromatic protons), 16.01 (s, NH) (**Fig. S5**); ^{13}C NMR (125 MHz, $CDCl_3$) (δ) 20.8, 28.6, 30.6, 52.8, 52.9, 118.7, 125.7, 132.4, 135.7, 136.1, 136.2, 137.0 (**Fig. S6**).

^1H NMR spectra of compounds CD1 and CD2, show a low field singlet, δ_{N-H} at around 15 ppm confirm strong intramolecular N–H…..O=C hydrogen bonding and the maximum dehielding of N–H proton is observed due to the presence of NO_2 at ortho position. Methyl substituents associated with the dimedone ring appear as a singlet at around 1.09 ppm as an average from rapidly inter-converting conformers. The methylene signals (2.62–2.64 ppm) also reflect rapid mobility of the dimedone ring. At room temperature the compound shows a set of signals observed for the methylene protons of dimedone ring and it indicates that the chemical shift difference is large enough to appear as a separate signal. In all the cases aromatic proton signals appear in the downfield region of 7.10–8.33 ppm with the expected splitting patterns.

For compounds CD1 and CD2, retention of a single signal for methyl groups at around 28 ppm denies any conformational preference. C-10, the carbon furthest from carbonyl groups, gives a single line at around 30.8 ppm and the upfield shift of around 20–22 ppm with respect to C-9 and C-11 is observed. Shielding differences for C-9 and C-11 carbons are observed in all the compounds. This is, perhaps, of some subtle geometry or electronic charge asymmetry within dimedone ring brought about by hydrogen bonding. Carbonyl sp^2 carbon atoms appear as separate signals in the low field region of about 197 and 193 ppm for C-12 and C-8, respectively. Strong intramolecular N–H……O–C hydrogen bonding deshields C-12 with respect to C-8 to the extent of ca. 4 ppm. Polarization changes of the carbonyl bond through p-conjugation with restricted rotation about N–N bond may well be accompanying factors for the observed deshielding. In general ^{13}C=N and ipso carbons are identified by their relative low intensities due to longer relaxation times and lower nuclear overhauser effects.

Single crystal X-ray diffraction studies

Single crystal of CD1 and CD2 were suitable for single crystal X-ray structure determination was obtained by recrystallization from ethanol, respectively. The crystal structures confirmed that the CD1 is methoxy substituted compound (Fig. 1) and CD2 is methyl substituted compound (Fig. 2). Crystal data: $C_{30}H_{34}N_6O_{10}$, Monoclinic, space group = C c, a = 23.380 (3) Å, b = 6.9690 (7) Å, c = 19.937 (3) Å, β = 110.851(15), V= 3035.7(7) $Å^3$, T = 293(2) K. The structure was solved by direct method with the SHELX program package. Positions of hydrogen atoms were located from electron difference density maps and refined isotropically. Full crystallographic parameters (excluding structure factors) for the structure in this paper have been deposited with the Cambridge Crystallographic Data Center as supplementary publication number CCDC 977177. Copies of the data can be obtained, free of charge, on application to CCDC, 12 Union Road, Cambridge CB2 1EZ, UK e-mail: deposit@ccdc.cam.ac.uk].

From the ORTEP diagram it is observed that the both phenyl and dimedone rings are twisted slightly about plane containing N2 and N1. Further the methoxy as well as nitro group are lying almost coplanar with the phenyl ring. The dimedone ring is found to pucker about C5-C4 and C7-C8 bonds to stabilize the strain in the molecule. In fig. 3, the intramolecular hydrogen bonding clearly shown in the packing diagram of CD1 compound.

A strong intramolecular hydrogen bond in CD1 (Fig. 3) molecule (D···A) C(16)-H(004)...O(5)#1, C(11)-H(006)...O(7)#2, N(5)-H(015)...O(4), N(5)-H(015)...O(11), N(2)-H(017)...O(5), N(2)-H(017)...O(6), C(15)-H(29)...O(3)#, C(16)-H(004)...O(5)#1, C(25)-H(005)...O(6)#4, C(11)-H(006)...O(7)#2, N(5)-H(015)...O(4), N(5)-H(015)...O(11), N(2)-H(017)...O(5), N(2)-H(017)...O(6), C(15)-H(29)...O(3)#3 distance are 3.230(6) , 3.427(5),

2.602(4), 2.628(4), 2.579(4), 2.622(4), 3.189(6), 3.230(6), 3.469(5), 3.427(5), 2.602(4), 2.628(4), 2.579(4), 2.622(4) and 3.189(6) respectively. The strong intramolecular hydrogen bonds are responsible for the stabilization of the molecules of CD1. The presence of nitro groups smooths the progress of the formation of additional hydrogen bonds (Table S2).

Scanning electron microscopy (SEM) was used to analyze the self-assembled microstructure of the resulting compounds. The morphologies of the hydrozone compound (CD1 and CD2) were observed to be different depending on the ligand group at para-position, i.e., OCH_3 and CH_3. Platinum was coated on the surface of samples and images of CD1 at 20, 5 and 2 μm are shown in fig. 4a, b and c respectively. The ligand CD1 shows a grass like structure and length of the -OCH_3 hydrozone around 11 μm length and 0.934 μm diameter (fig. 4c). The ligand CD2 illustrated microrods like structure of size 15.306 μm and 0.36 μm (Fig. 5a, b and c). We observed considerable change in the ligands morphology when cobalt ion was added to them (i.e. in the complex). The complex of CD1 with Co^{2+} ion, shows the grass covered with large amount spherical particles like surface morphology (Fig. 6a and b), but their size was relatively different. The complex of CD2 with Co^{2+} ion, shows self-assembled microsheets (Fig. 7a and b).

Solvatochromism and chemosensor

The solvatochromic properties of these novel compounds were evaluated using compounds CD1 and CD2 (Fig. 8A and B) absorbs in the longest wavelength region, as models. For this, spectra were recorded in 15 solvents having different polarities. Although individual bands in the spectra are commonly overlapped (see, for example, the absorption spectrum of CD1 (Fig. 8), they could be resolved after applying a smoothing spline algorithm to the observed data followed by a derivative spectroscopy numerical method (only the negative peaks of the

second derivatives of the smoothed spectra were used for the estimation of the position of the bands). The maximum absorbance corresponds to n → π* transition of the azo group of the CD1 and CD2 in ethanol due to the internal charge transfer event of the azo chromophore from donor to acceptor (push–pull effect).

The fluorescence spectra of two derivatives were measured in 15 solvents at room temperature (Fig. 8b and d). The spectral shapes are broad without any vibronic structure. The trends are quite clear. There is a moderate bathochromic (5-10 nm) shift observed in derivatives. Both electrondonating and electron-withdrawing substituents in the para position of hydrazonyl moiety cause a significant bathochromic (12 nm) shift with respect to parent compounds. The hydrozones are essentially shown slight positive solvatochromism in polar solvents. The longest wavelength maxima were found in DMSO, although the latter shows a lower dielectric constant than acetonitrile. This probably some specific solute-solvent interaction (e.g. H-bonding) moderately affects the position of spectral maxima. This bathochromic shift of the absorption band, which corresponds with a n-π * electronic spectral transition, is related to a greater stabilization of the excited state relative to the ground state with increasing polarity of the solvent.

Fluorescence emission spectroscopy was used to monitor the competition event. The fluorescence enhancement observed for Co^{2+} (CD1 and CD2). Upon addition of Co^{2+} ions to CD1 and CD2 in ethanol, an enormous fluorescence enhancement is observed at 548 and 490 nm respectively (Fig. 9A and 9B). The fluorescence enhancement observed for Co^{2+} is not seen for other metal ions, such as Zn^{2+}, Cu^{2+}, Pb^{2+}, Hg^{2+}, Cr^{3+}, Na^{+}, K^{+}, Mg^{2+}, Ni^{2+}, Fe^{2+}, Fe^{3+}, Al^{3+}, Cd^{2+} and Ag^{+} (Fig. 9). Ni^{2+} does cause some fluorescence enhancement. A variety of metal ions were tested and many, such Zn^{2+}, Cu^{2+}, Pb^{2+}, Hg^{2+}, Cr^{3+}, Na^{+}, K^{+}, Mg^{2+}, Ni^{2+}, Fe^{2+}, Fe^{3+}, Al^{3+}, Cd^{2+} and

Ag^{+} had little effect when one equivalent was added. When more equivalents of Zn^{2+}, Cu^{2+}, Pb^{2+}, Hg^{2+}, Cr^{3+}, Na^{+}, K^{+}, Mg^{2+}, Ni^{2+}, Fe^{2+}, Fe^{3+}, Al^{3+}, Cd^{2+} and Ag^{+} were added, some reduction in the fluorescence was observed. This implies that these metal ions are displacing the Co^{2+} from CD1 and CD2.

To understand the interaction between compound CD1, CD2 and Co^{2+}, the fluorescence variation of compounds CD1, CD2 were measured upon the addition of Co^{2+} from 0 to 10 μM (Fig. 10) at neutral pH. Their fluorescence spectra are the same when normalized. However, the UV-vis absorption spectrum of compounds CD1, CD2 shifts 6 nm to the blue when 15 μM of Co^{2+} is introduced. These results reveal the certain structural modification on compound 1 by adding Co^{2+}, indicative of fluorescence enhancement induced by binding Co^{2+}. So that we have limited with 10 μm and the limit of detection (LOD) were 3 μm to 7 μm (**Fig. S9**). Beyond that the fluorescence intensity start to decrese. Furthermore, it is well-known in coordination chemistry that the complexation of cobalt with a ligand containing at least two nitrogen donor atoms is favored by the activation of the inert pair on the Co^{2+} ion, leading to a shortening of the Co–N bond length and a much stronger covalent bonding.

To further investigate the selectivity for Co^{2+} ions over other metal ions, interferences to the selective response of receptor CD1 and CD2 to Co^{2+} by coexisting ions were evaluated, no significant interference in detection of Co^{2+} was observed in the presence of other competitive cations. These results suggested that CD1 and CD2 can be used as a potential chemosensor for the Co^{2+} ion. Their fluorescence spectra are the same when normalized. As shown by the figures, there is a smooth transition from the free compound to the Co^{2+} bound complex. A red shift of absorption peaks is often observed when Co^{2+} bind to compounds. The absorption values tails off into the visible and thus would allow CD compounds to be excited in the visible light region.

In addition, the spectroscopic responses were reversible when the Co^{2+} chelating reagent $EDTANa_2$ (1.0 equiv.) was added to CD1–Co^{2+} and CD2–Co^{2+} solution, the fluorescence spectrum almost revived to the original shape of free CD1 and CD2, which indicate the effective Co^{2+} removal. The phenomenon proves that these compounds could serve as a selective "on-off" sensor for Co^{2+}. (Fig. 11)

pH-Dependent Behavior

The influence of pH on chemosensor CD1 and CD2 were studied using UV-vis-spectrocopy (**Fig. S9**). Over a pH range of 3-9, the visible absorption band centered at 444 nm in CD1 and 426 nm in CD2 were unchanged. But increase in pH from 9 to 11 engendered a shift in the maximum absorption wavelength to 355 nm (CD1) and 354 nm (CD2) with color change of yellow to pink. This difference were due to the dissociation of CD1-Co^{2+} and CD2-Co^{2+} complex, which result in lower absorbance and color change. The pH emission spectra of CD1 and CD2 (**Fig. S10**) were monitored and showed significant changes in emission intensity in the range of 3-11.The emission intensity of CD1 and CD2 with Co^{2+} increased dramatically from pH 3 to 5, resulting from the competition between the N-H proton and Co^{2+} ion[28, 29]. In particular, slight significant change in fluorescence spectra were observed in the range of pH 5-9 and decresed under alkaline condition with a color change of yellow to pink .The quenching at higher pH could be well explained by the formation of $Co(OH)_2$ and thus reducing the concentration of Co^{2+} - CD 1/ CD2 [30]. From the above result it has been shown that the effect of pH on CD 1 / CD 2-Co^{2+} were exhibited stable fluroscence intensity at a pH range from 5 to 9. Since we have carried out CD1 and CD2 compounds in neutral limits.

Natural bond orbital analysis

NBO analysis of calculations B3LYP/6-31G was carried out for the compound CD1 and CD2. The important second order perturbative estimates of donor-acceptor interactions are displayed in table 3. This is mainly due to the strong intramolecular hydrogen bonding between O9 and H33.Then the delocalization of N12 electrons from C13-C14 bond to C15-C16 bond and C13-C14 bond to C15-C16 bond. Among these two C13-C14 bonds to C17-C18 bond delocalization energy is high due to electron withdrawing group (NO_2) is present at ortho position of the phenyl ring. The delocalization energy corresponding to the intramolecular hydrogen bonding is slightly lower in CD1 than in CD2.

In compound CD1 and CD2 the N7-N12 and N12-C13 bond lengths are1. 316, 1.393, 1.318, 1.384 A° and 1.32, 1.409, 1.269, 1.321 A° by the experimental measurements using Single crystal X-ray diffraction studies (SCXRD) and theoretical (DFT), respectively, it shows that a single-bond character. C5-N7 bond lengths of 1.315, 1.31 A° and 1.334 A°, 1.33 A° for experimental and theoretical values (in CD1 and CD2 respectively) are indicative of a significant double-bond character of C5-N7. The C4-O9 bond distance in CD1 and CD2 were 1.222 A°, 1.225 A° by SCXRD and 1.269 A°, 1.243 A° by DFT, consistent with the value of the carbonyl compound i.e. C=O[31-35]. C6-C5-N7-N12, N7-N12-C13-C14 and C5-N7-N12-C13 torsion angles were 178.9,-0.3, 169.6, -1.1,-178.5, 179.1 by SCXRD and 179.1, 179, 169.6, 142.2, 175.7, 176.2 by DFT respectively (Table 4). When we compare the table 4 values, between the calculated and observed geometrical parameters, there were some differences. Since the experimental results were obtained from in the solid state while the theoretical results were based on an isolated molecule in the gaseous phase, these differences were not unforeseen. The optimized structural parameters can well reproduce the literature values. The small difference between the computed

data is due to calculation belongs to gaseous phase and the experimental result belong to solid phase.

Molecular orbital studies

The HOMO-LUMO energies were also calculated and the values and fig. 12 are listed in table 5. The highest occupied molecular orbital (HOMO) and the lowest unoccupied molecular orbital (LUMO) are the main orbital's that take part in chemical stability[36]. The HOMO represents the ability to donate an electron, LUMO as an electron acceptor represents the ability to obtain an electron. HOMO→LUMO transition implies an electron density transfer to nitro group from OCH3 in CD1 and CH3 group in CD2. The value of energy separation between the HOMO and LUMO are 3.3733 (CD1) and 3.555 (CD2). The chemical hardness and softness of a molecule is a good indication of the chemical stability of a molecule. From the HOMO–LUMO energy gap, one can find whether the molecule is hard or soft. The molecules having a large energy gap are known as hard, and molecules having a small energy gap is known as soft molecules. The soft molecules are more polarizable than the hard ones, because they need small energy for excitation. The hardness value of a molecule can be determined by the formula[37].

$$\eta = \frac{\varepsilon_{HOMO} + \varepsilon_{LUMO}}{2}$$

Where εHOMO and εLUMO are the energies of the HOMO and LUMO molecular orbitals. The value of η (Hardness) of the CD1 and CD2 molecule are 1.6866 eV and 1.7775 eV. Hence, from the calculation; we conclude that the molecules were taken under investigation belongs to the hard materials orbital. HOMO and HOMO-1 are characterized as a π-bonding molecular orbital and the LUMO and LUMO+1 exhibit a π* molecular orbital. .

Vibrational frequencies for the minimum energy conformer was also calculated by DFT method. These values were corrected using scale factor 0.962 and the corrected frequencies and proposed assignments were summarized in table 7 along with the observed values. These values indicate that there is a close agreement between the calculated values and observed values.

Molecular electrostatic potential (MEP) maps

To predict reactive sites for electrophilic and nucleophilic attack for the investigated molecule, MEP is calculated (red is negative, blue is positive) at the 3LYP/6−31G optimized geometries. Fig. 13 shows the calculated 3D electrostatic potential contour map of CD1 and CD2 .The different values of the electrostatic potential at the surface are represented by different colors. Potential increases in the order red < orange < yellow < green < blue. The color code of these maps is in the range between $-7.977e^{-2}$ (deepest red) to 7.977 e^{-2} (deepest blue) in compound CD1 and $-7.886e^{-2}$ (deepest red) to 7.886 e^{-2} (deepest blue) in compound CD2, where blue indicates the strongest attraction and red indicates the strongest repulsion. From this result, it is clear that the H atoms indicate the strongest attraction and O atoms indicate the strongest repulsion.

Charge distribution

The charge distribution of the molecule has been calculated on the basis of Mulliken method using a B3LYP/6-31G level calculation. This calculation depicts the charges of the every atom in the molecule. Distribution of positive and negative charges is the vital to increasing or decreasing of bond length between the atoms. Mulliken atomic charges and the plot has shown in table 6 and Fig. 14. The Mulliken scheme places the negative charge more or less evenly on C1,C2, C3, C7, C8, C9, C10,C11, N12, C14, C15, C17, O20, O21, O22, C23 atoms and N7, O8, O9, N12, O20, O21 atoms in compound CD1 and CD2 respectively and splits the positive

charge among the all hydrogen atom and some of the C4, C5, C6, C13, C16, C18, N19 atoms in CD1 and C1, C2, C3, C4, C5, C6, C10, C11, C13, C14, C15, C16, C17, C18, C19 atoms in CD2 Mulliken population analysis compute charges by dividing orbital overlap evenly between the two atoms involved.

Conclusions

In summary, the hydrazones of β-diketones have been synthesized and characterized IR, ^{1}H, ^{13}C NMR spectra and Single crystal X-ray diffraction studies. The FT-IR, NMR, A single crystal X-ray diffraction study data clearly shows the effective intramolecular hydrogen bonding in all synthesized substituted hydrazones. Packing diagram explains the strong intramolecular hydrogen bonding in CD1 and CD2 molecule. A promising analytical approach for detecting Co^{2+} in aqueous solutions at neutral pH with a detection limit of 3μm to 7μm. When a cobalt ion was added in CD1 and CD2 their morphological changes were observed. We have prepared a simple type of fluorescent "on-off" chemosensor based on hydrazones shows interesting properties such as high sensitivity for Co^{2+}. It possesses a high affinity and selectivity for cobalt ions relative to most other competitive metal ions by enhancement of the monomer fluorescence emission of hydrazones in organic aqueous solution. We expect that the present design strategy and the remarkable photophysical properties of this sensor will help to extend the applications of fluorescent sensors for metal ions. In this present investigation, molecular structure, HOMO, LUMO, NBO, Mulliken charges and MEP analysis have been studied using ab initio DFT B3LYP/6-31G calculation.

References

1 G. Sivaraman, T. Anand and D. Chellappa, *Analyst*, 2012, **137,** 5881.

2 G. Sivaraman, T. Anand and D. Chellappa, *Anal. Methods*, 2014, **6,** 2343

3 T. Anand , G. Sivaraman, P. Anandh, D. Chellappa and S. Govindarajan, *Tetrahedron Lett.,* 2014, **55,** 671–675.

4 G. Sivaraman, V. Sathiyaraja and D. Chellappa, *J. Lumin.,* 2014, **145,** 480.

5 G. Sivaraman, T. Anand and D. Chellappa, *RSC Advances* (DOI: 10.1039/c3ra42109k).

6 C.Y. Li, X. B. Znang, Z. Jin, R. Hari, G. L. Shen and R.Q. Yu, *Anal. chim. Acta.,* 2006, **580**, 143.

7 C. Reimann, F. Koller, G. Kashulina and H. P. Englmaier, *Environ.Pollut.,* 2001, **115**, 239.

8 I. Mori, K. Takasaki, Y. Fujta and T. Matsin, *Talanta* 1998, **47**, 631.

9 F. Monteil Rivera and J. Dumonceau, *Ana. Bioanal.Chem.,* 2002, **374**, 1105.

10 M. Montalti, L. Prodi and N. Zaccheroni, *J. Mater.Chem.,* 2005, **15**, 2810.

11 F. R. Pavan, P. I. S. Maia, S. R. A. Leite, V. M. Deflon, A. A. Batista, D. N. Sato, S. G. Franzblau and C. Q. F. Leite, *Eur. J. Med. Chem.,* 2010, **45,** 1898.

12 X. Su and I. Aprahamian, *Chem. Soc. Rev.,* 2014, **43**, 1963.

13 G. Gilli and P. Gilli, The Nature of the Hydrogen Bond: Outline of a Comprehensive Hydrogen Bond Theory, Oxford University Press, Oxford, 2009.

14 P. Gilli and G. Gilli, *J. Mol. Struct.*, 2010, **972**, 2.

15 M. N. Kopylovich, K. T. Mahmudov, M. Archana and A. J. L. Pombeiro, *Chem. Commun.,* 2011, **47**, 7248.

16 K. T. Mahmudov, A. M. Maharramov, R. A. Aliyeva, F. M. Chyragov , R. K. Askerov , P. Q. Hasanov , M. N. Kopylovich and A. J. L. Pombeiro, *J. Mol. Struct.*, 2011, **1006** , 576.

17 K. T. Mahmudova, M. N. Kopylovich and A. J. L. Pombeiro, *Coord. Chem. Rev.,* 2013, **257**, 1244.

18 A. Sethukumar and B. A. Prakasam, *J. Mol. Struct.*, 2010, **963,** 250.

19 J. Griffiths, J. Soc. *Dyers Colour.,* 1972;**88**, 106.

20 M. H. R. Bartel, *J. Prakt. Chem.,* 1982, **324**, 743.

21 P. Nikolov, F. Fratev, S. Stoyanov and O. E. Polansky, *Z. Naturforsch., B: Chem. Sci.* 1981, **36,** 191.

22 H. Joshi, F. S. Kamounah, C. Gooijer, G .V. D. Zwan and L. Antonov, *J. Photochem. Photobiol. A,* 2002, **152**, 183.

23 T. Aysha, S. L. Jr., A. Lycka and R. Hrdina, *Dyes Pigm.,* 2011, **91,** 170.

24 B. W. Lin, L. Yuan, L. Long, C. Guo, and J. Feng, *Adv. Funct. Mater.*, 2008, **18,** 2366.

25 A. K. Mahapatra, S. K. Manna, D. Mandal and C. D. Mukhopadhyay, *Inorg. Chem.,* 2013, **52**, 10825.

26 Gaussian 03 Program, Gaussian Inc., Walling ford CT, 2004.

27 H. B. Schlegel, *J. Comput. Chem.,* 1982, **3** 214.

28 L. Xue, G. P. Li, D. J. Zhu, Q. Liu and H. Jiang, Inorg. Chem., 2012, 51, 10842.

29 Y. Zhang, X. F. Guo, W. X. Si, L. H. Jia, X. H. Qian, Org. Lett., 2008, 10, 473.

30 X. Y. Zhou, B. R. Yu, Y. L. Guo, X. L. Tang, H. H. Zhang and W. S. Liu, Inorg. Chem., 2010, 49, 4002.

31. L. J. Huang, G. H. Kuhn, V. N. Nesterov, B. B. Averkiev, B. Penn, M. Yn. Antipin, T.V. Timofeeva, *Acta Cryst.,* 2002, **C58**, o624.

32 B. Kosar, C. Albayrak, M. odabasoglu and O.Buyukgungor, *Acta Cryst.*, 2004, **E60**, 190.

33 T. S. Basu-Baul, S. Kundu, H. D. Arman and E.R.T. Tiekink, *Acta Cryst.,* 2009, **E65**,3061.

34 B. Minisini, G. Fayet, F. Tsobnang and J.F.Bardeau, *J. Mol. Model.* 2007, **13**, 1227.

35 S. Yazic, C. Albayrak, ˙I. E. gumrukcuoglu, I. Senel and O. Buyukgungor, *Turk. J. Chem.* 2011, **35**, 341.

36 S.Gunasekaran, R.A. Balaji, S. Kumaresan, G. Anand, S. Srinivasan, *Can. J. Anal. Sci. Spectros.* 2008, **53,**149.

37 K. Fukui, *Science,* 1982, **218**, 747.

Figure captions and Scheme

Fig. 1 ORTEP of compound CD1.

Fig. 2 ORTEP of compound CD2.

Fig. 3 Packing diagram of CD1 (Hydrogen bonding).

Fig. 4 SEM images of CD1 (a) 20 µm, (b) 5 µm and (c) 2 µm.

Fig. 5 SEM images of CD2 (a) 50 µm, (b) 5 µm and (c) 1 µm.

Fig. 6 SEM images of CD1 with Co^{2+} (Complex) (a) 20 µm and (b) 5 µm.

Fig. 7 SEM images of CD2 with Co^{2+} (Complex) (a) 20 µm and (b) 5 µm.

Fig. 8 UV and Emission spectra of CD1 andCD2 in different solvents.

Fig. 9 Fluorescence emission spectra of 10µm solutions chemosensors for CD1(A) with different metal ions (perchlorate, chloride, or nitrate salts of (a) Co^{2+}, (b) Ni^{2+}, (c) Cu^{2+}, (d) Zn^{2+}, (e) Pb^{2+}, (f) Hg^{2+}, (g) Mg^{2+}, (h) Cr^{3+}, (i) Na^{+}, (j) K^{+}, (k) Fe^{2+}, (l) Fe^{3+}, (m) Al^{3+}, (n) Cd^{2+} and (o) Ag+) in aq CH_3CH_2OH (CH_3CH_2OH/H_2O = 4/1, v/v, 10 µM HEPES buffer, pH = 7.0).

(B) Fluorescence emission spectra of 10µm solutions chemosensors for CD2 with different metal ions (perchlorate, chloride, or nitrate salts of (a) Co^{2+}, (b) Ni^{2+}, (c) Cu^{2+}, (d) Zn^{2+}, (e) Pb^{2+}, (f) Hg^{2+}, (g) Mg^{2+}, (h) Cr^{3+}, (i) Na^{+}, (j) K^{+},(k) Fe^{2+}, (l) Fe^{3+}, (m) Al^{3+}, (n) Cd^{2+} and (o) Ag+) in aq CH_3CH_2OH (CH_3CH_2OH/H_2O = 4/1, v/v, 10 µM HEPES buffer, pH = 7.0).

Fig. 10 Emission spectra of compound CD1 (A) and CD2 (B) in the presence of an increasing Co^{2+} concentration (0-10 µm)in ethanol solution.

Fig. 11 Fluorescence spectra of CD1 and CD2 +Co^{2+}, cd1 and CD2 + Co^{2+}+EDTANa2 in ethanol solution.

Fig. 12 HOMO, LUMO energy diagram of CD1 and CD2.

Fig. 13 Molecular electrostatic potential surface (MEP) of CD1 and CD2.

Fig. 14 Mulliken atomic charges for CD1 & CD2

Scheme 1 Schematic representation of synthesis of Hydrozone .

Table 1. Absorbtion fluorescence and stoke shift values of CD1 and CD2.

Table 2. Crystal data, data collection and structure refinement for CD1 and CD2.

Table 3. NBO analysis of CD1 & CD2 by DFT method (B3LYP/6-31G).

Table 4. Experimental and theoretical values comparison (Bond length, Bond angle and torsion angle ^{o}).

Table 5. Calculated HOMO-LUMO energies (eV) 0f CD1 and CD2.

Table 6. Mulliken atomic charges for CD1 & CD2.

Table 7.Theoretical and experimental IR spectral data (cm^{-1}) of compound CD1 & CD2.

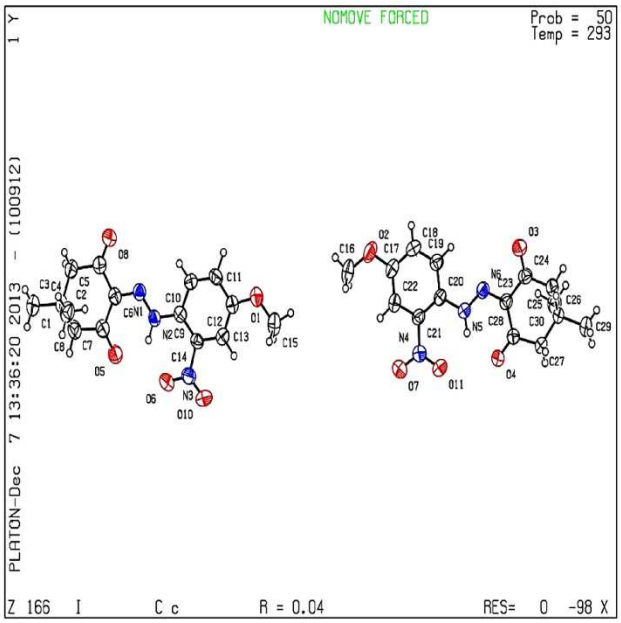

Fig. 1

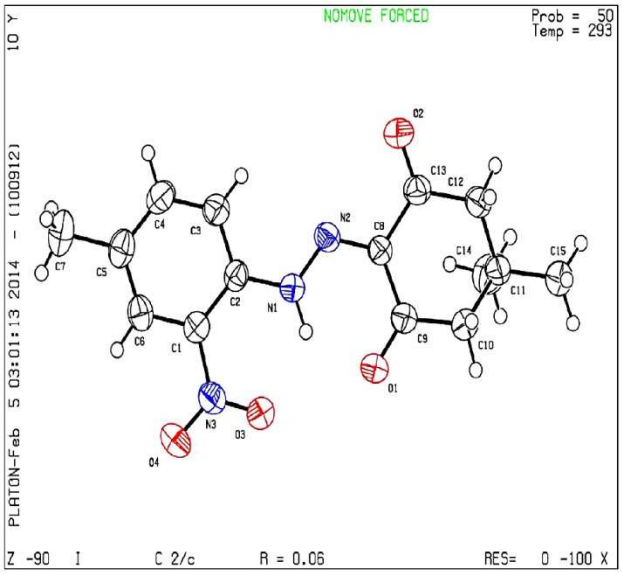

Fig. 2

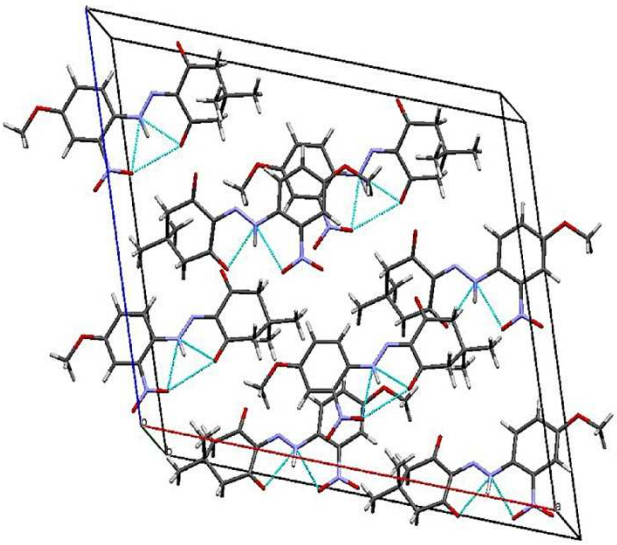

Fig. 3

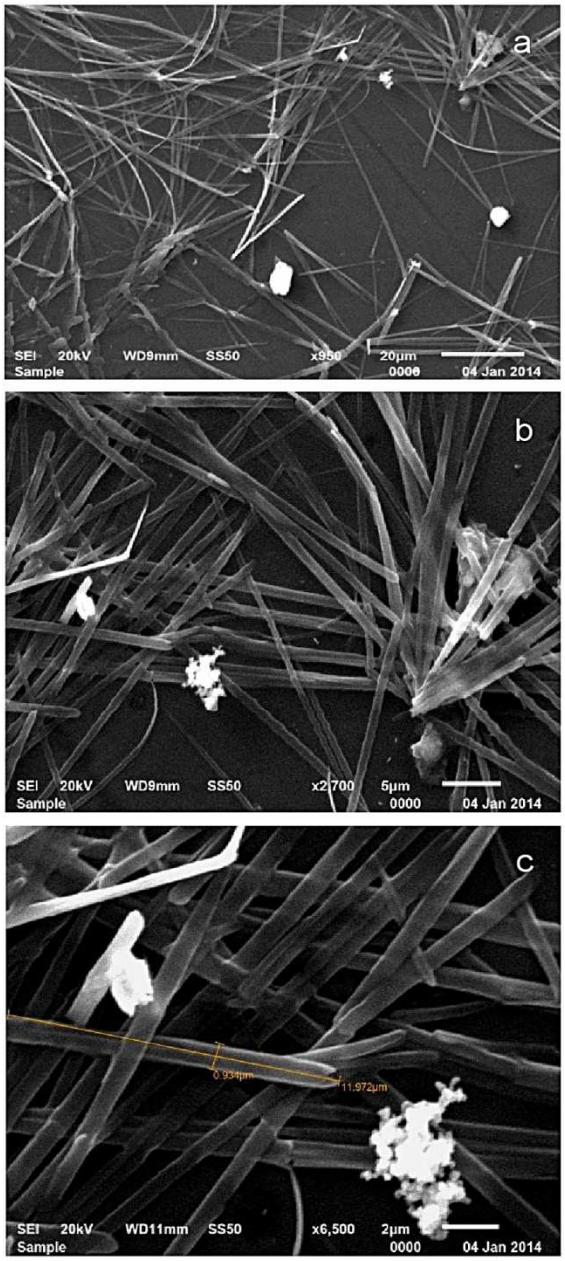

Fig. 4

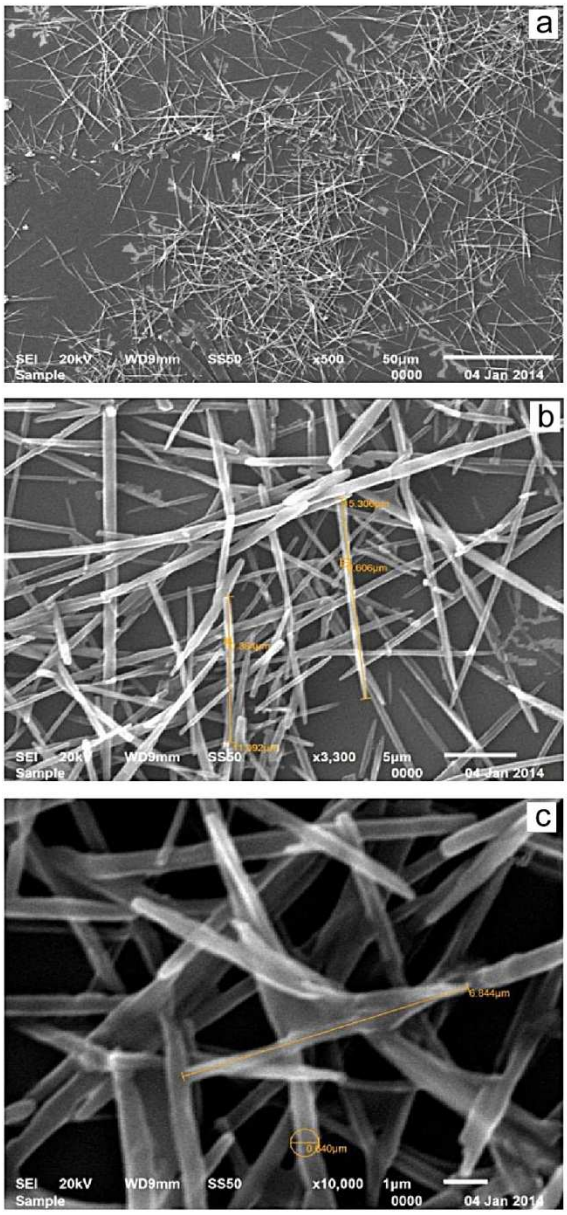

Fig. 5

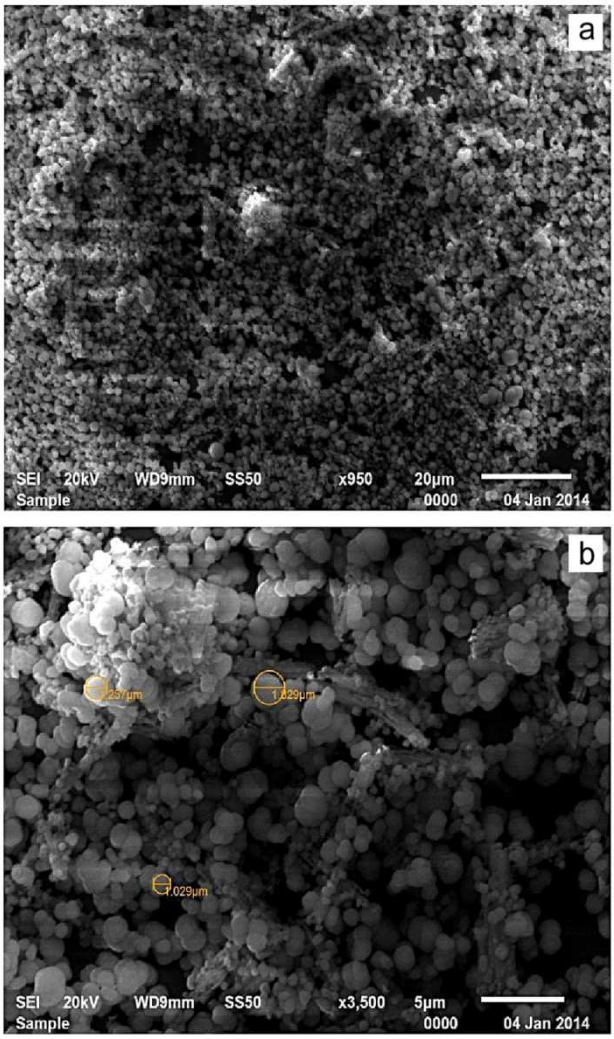

Fig. 6

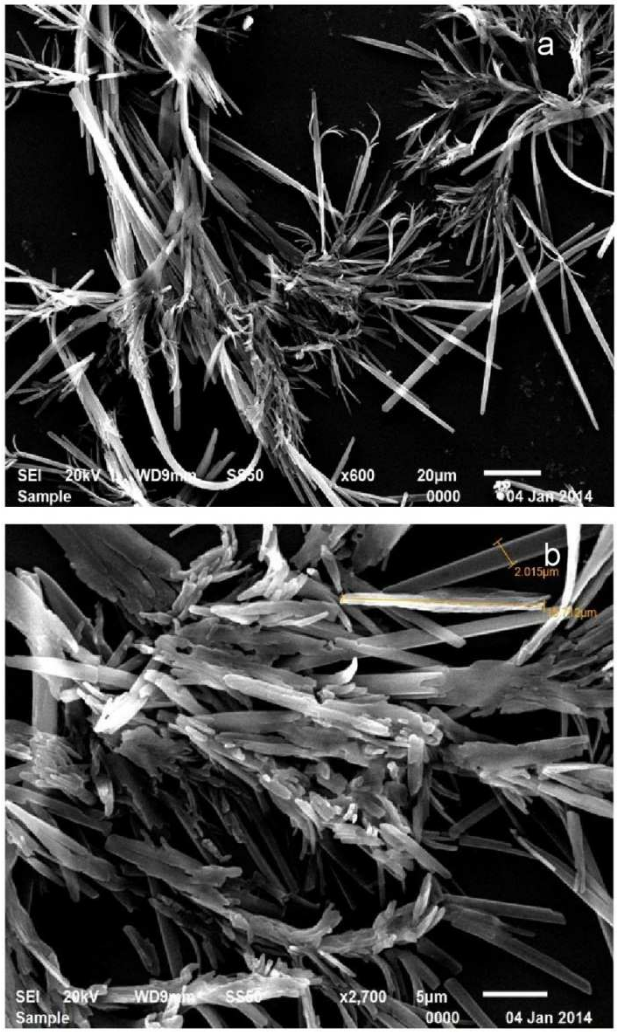

Fig. 7

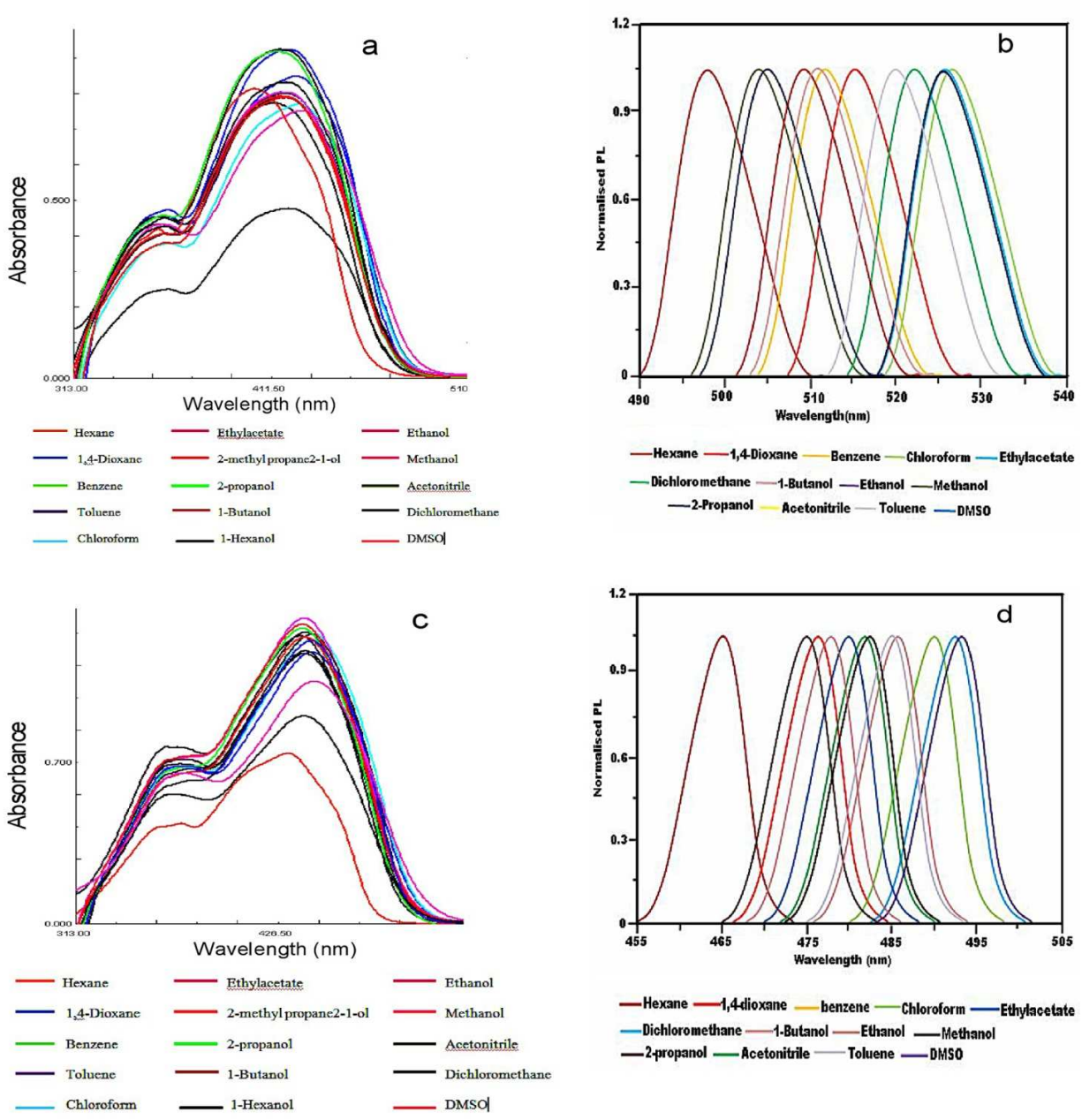

Fig. 8

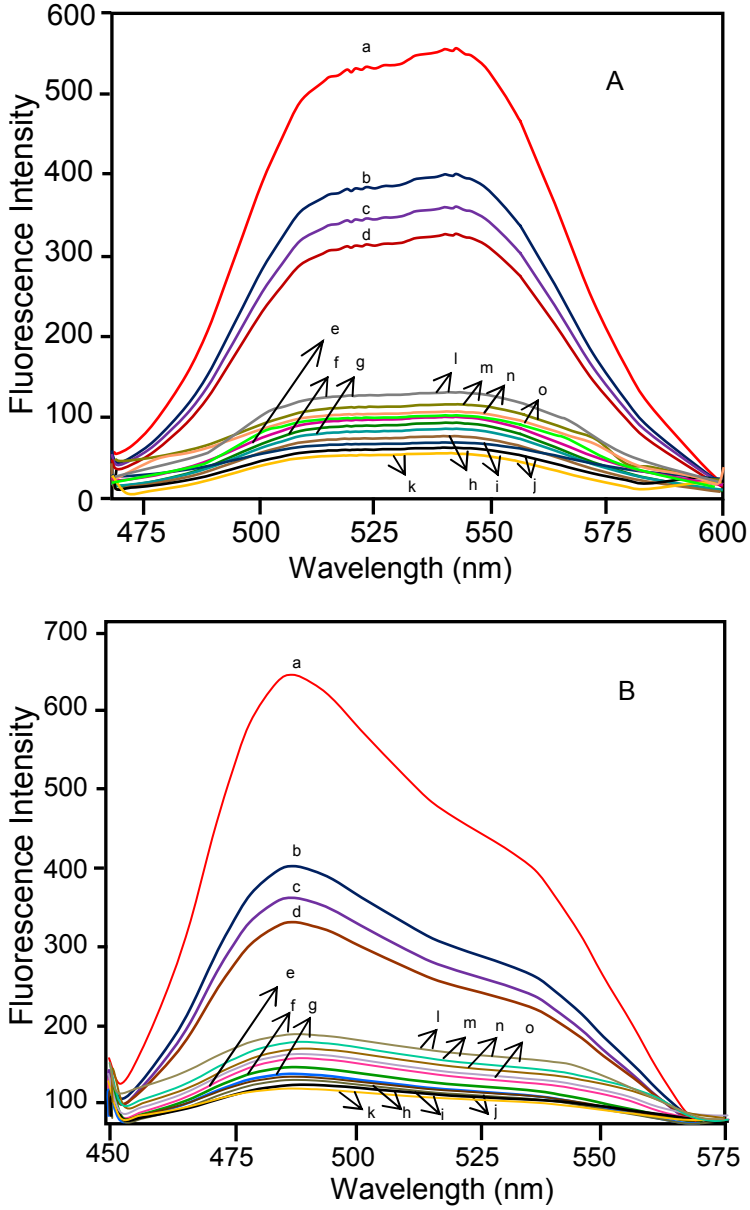

Fig. 9

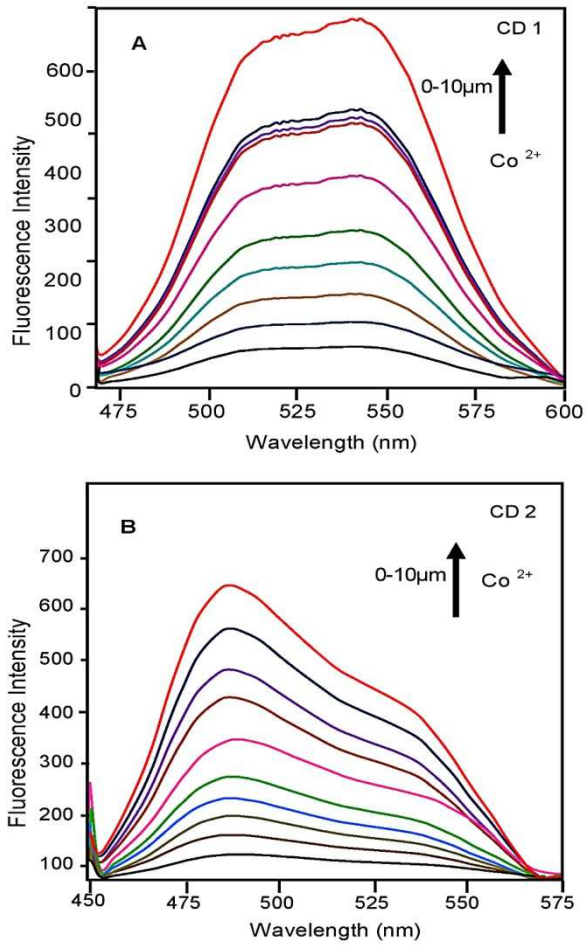

Fig. 10

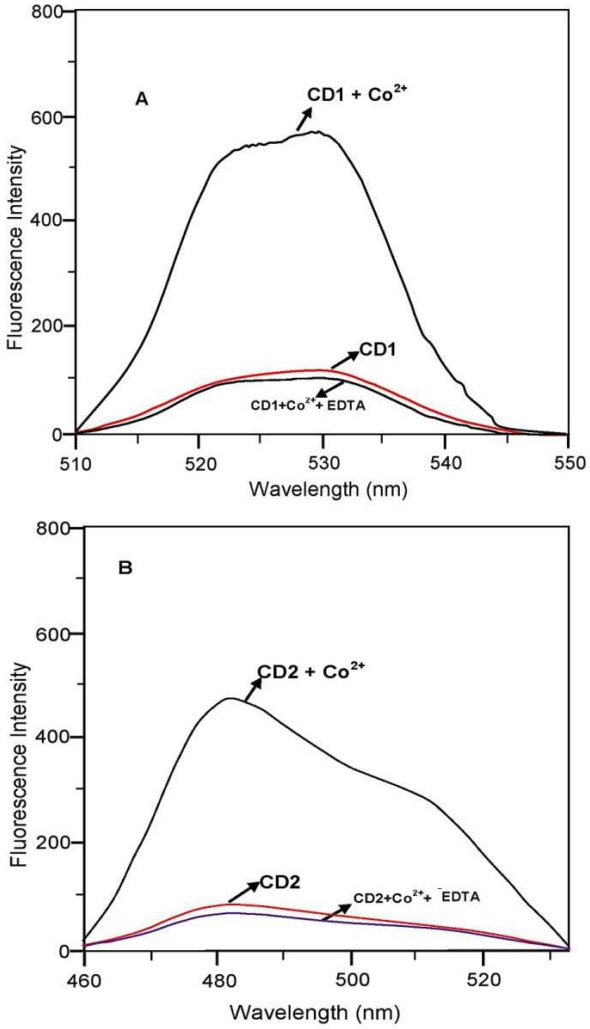

Fig. 11

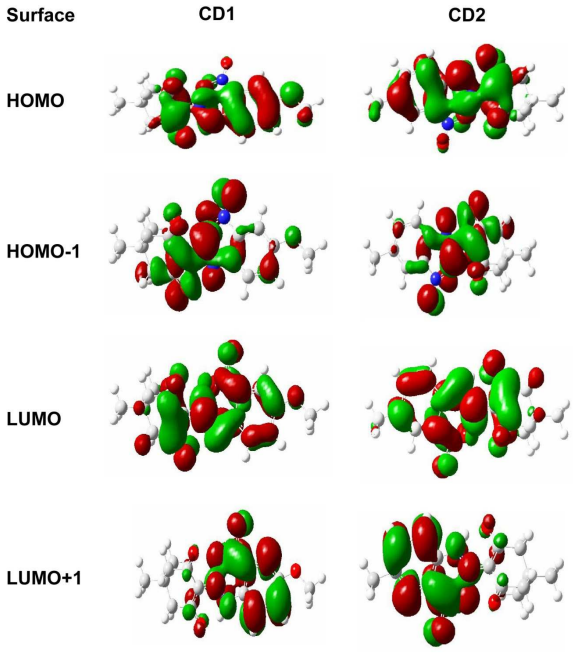

Fig. 12

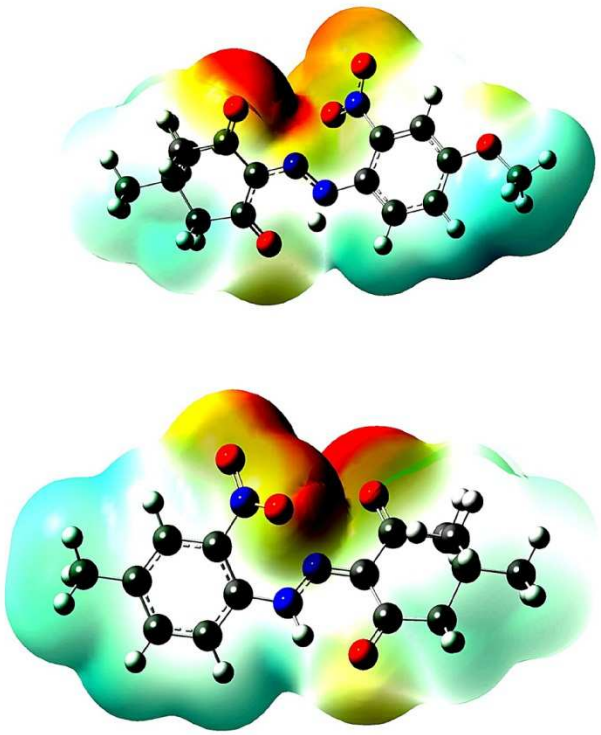

Fig. 13

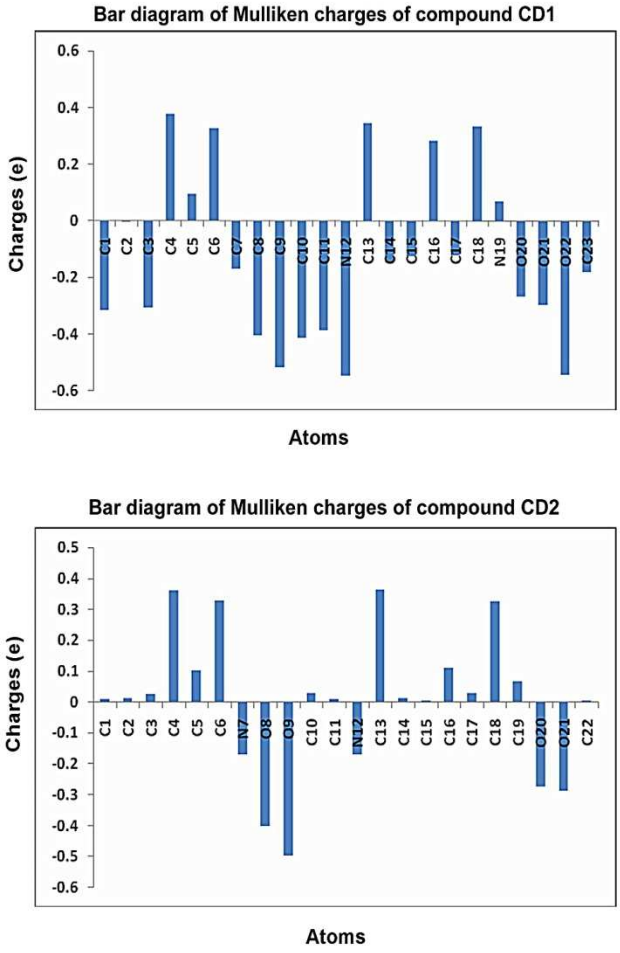

Fig. 14

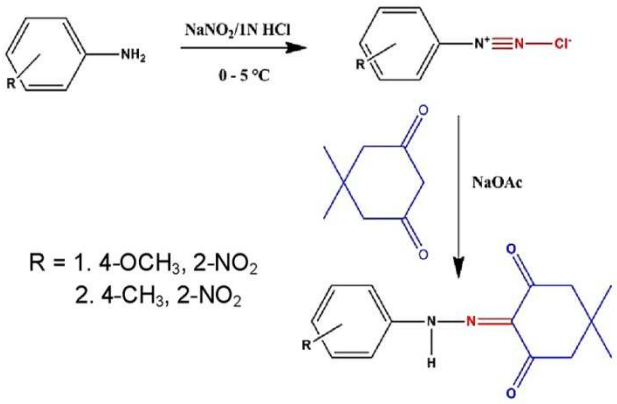

Scheme 1

S.No	CD 1			CD 2		
Solvent	Obs	FL	$\Delta\nu_{st}$ cm^{-1}	Obs	FL	$\Delta\nu_{st}$ cm^{-1}
Hexane	431	498	3121.535	403	465	3308.519
1,4-dioxane	441	516	3295.892	416	477	3074.101
Benzene	444	512	2991.273	420	483	3105.59
Chloroform	446	527	3446.193	424	490	3176.742
2-propanol	440	515	3309.797	414	475	3101.958
1-butanol	441	511	3106.265	416	478	3117.959
Ethanol	441	526	3664.33	416	486	3462.33
Methanol	439	519	3511.221	416	483	3334.528
Acetonitrile	440	519	3459.45	416	482	3291.574
DCM	445	523	3351.451	423	493	3356.686
DMSO	447	526	3359.958	426	498	3393.857
Ethylacetate	438	526	3819.643	413	480	3379.742
Toluene	444	520	3291.753	420	485	3190.967
1-Hexanol	442	515	3206.959	416	481	3248.441
2-Methyl propane 1-ol	441	519	3407.914	413	480	5344.68

Table 1

	CD 1	**CD2**
Empirical formula	C_{30} H_{34} N_6 O_{10}	C15 H17 N3 O4
Formula weight	319.0	303.3
T (K)	293(2)	293(2)
Wavelength (Å)	0.71073	0.71073 A
Crystal system, space group	Monoclinic, C c	Monoclinic, C 2/c
Unit-cell dimensions		
a (Å)	23.380(3)	21.628(5)
b (Å)	6.9690(7)	6.8734(11)
c (Å)	19.937(3)	21.792(5)
β (°)	110.851(15)	115.39(3)
Volume ($Å^3$)	3035.7(7)	2926.7(12)
Z, Calculated density D (mg/m^3)	57, 1.397	41, 1.417
Absorption coefficient μ (mm^{-1})	0.107	0.133
F(000)	1344	1248
h range for data collection (°)	3.068 to 29.062	3.142 to 27.992
hkl range	-26<=h<=31	-11<=h<=28
	-5<=k<=9	-4<=k<=8
	-19<=l<=26	-28<=l<=26
Reflections		
Reflections collected	25.242	27.992
Unique R_{int}	4217 (0.0227)	3275 (0.0288)
Observed	6184	5809
Data / restraints / parameters	4217 / 2 / 552	3275 / 0 / 267
Goodness-of-fit on F^2	1.036	1.038
Absolute structure parameter R(F) (I > 2σ(I))	0.1(7)	0.1004
Extinction coefficient wR(F^2) (all data)	0.0010(2)	n/a
Largest diff. peak and hole Max/min.Δ σ($e/Å^3$)	0.182 /-0.145	0.210/-0.225

Table 2.

NBO analysis of CD1 & CD2 by DFT method (B3LYP/6-31G			
Donar NBO BD(2)	Acceptor NBO BD*(2) /LP	CD1	CD2
C5 - N7	C4 - O9	23.73	23.41
C5 -N7	C6 - O8	17.6	17.37
C13-C14	C15 - C16	18.37	-
C13 - C14	C17 - C18	19.9	-
C15 - C16	C13 - C14	22.15	-
C15- C16	C17 - C18	20.2	-
C17- C18	C13 - C14	18.95	-
C17- C18	C15 - C16	18.52	-
C17 - C18	N19 - O21	21.62	-
N12-C13	C5-N7	-	36.11
C14-C15	N12-C13	-	35.7
C14-C15	C16-C17	-	18.79
C16-C17	C14-C15	-	20.6
LP (2) O8	BD*(1)C1 - C6	17.77	17.78
LP (2) O8	BD*(1) C5 - C6	20.27	20.39
LP (2) O9	BD*(1) C3 - C4	15.74	15.79
LP (2) O9	BD*(1) C4 - C5	10.8	10.25
LP (1) N12	BD*(2) C5 - N7	49.93	-
LP (1)N12	BD*(2) C13 - C14	14.43	-
LP (2)O20	BD*(1) C18 - N19	11.03	10.7
LP(2)O20	BD*(1) N19 - O21	18.34	18.3
LP (3)O20	BD*(2) N19 - O21	155.5	152.36
LP (2)O21	BD*(1) C18 - N19	11.32	11.16
LP (2)O21	BD*(1) N19 - O20	18.27	18.39
LP (2) O22	BD*(2) C15 - C16	30.86	-
LP(2)09	BD* (1)N12-H33	-	16.59
LP(1)C18	BD*(2)N12-C13	-	280.6
LP(1)C18	BD*(2)C16-C17	-	58.49
LP(1)C18	BD*(2)N19-O21	-	393.59

Table 3

	CD1		CD2	
	Experimental	**Theoretical**	**Experimental**	**Theoretical**
Bond length (A°)				
C5-N7	1.315	1.334	1.31	1.333
C6-O8	1.211	1.244	1.21	1.243
C4-O9	1.231	1.27	1.225	1.269
N7-N12	1.316	1.32	1.318	1.321
N12-C13	1.393	1.409	1.384	1.407
C18-N19	1.215	1.471	1.453	1.469
N19-O20	1.221	1.261	1.218	1.263
N19-O21	1.215	1.261	1.221	1.261
C16-O22	1.351	1.382	-	-
O22-C23	1.426	1.455	-	-
N12-H34	0.94	1.03	0.92	1.031
Bond angle(°)				
C5-N7-N12	119	120.9	118.7	120.9
O21-N19-O20	121.6	124.5	122.3	124.4
C16-O22-C23	117.7	119.1	-	-
N7-N12-C13	119.3	119.9	120.2	120.1
C13-N12-H34	118	122.1	121	121.9
N7-N12-H34	119.3	117.8	118.8	117.9
O8-C6-C5	121.7	122.5	120.5	122.5
O8-C6-C1	121.5	120.5	121.1	120.5
O8-C6-C1	114.7	115.6	125	115.6
N7-C5-C4	124.8	123.3	115.5	123.3
O9-C4-C5	121.1	121	121.2	120.9
O9-C4-C3	120.5	119.6	120.9	119.6
C17-C18-N19	115.7	116	116.3	116.2
C13-C18-N19	122	122.5	121.8	122.7
N12-C13-C14	120.1	118.2	120.4	117.9
N12-C13-C18	123.4	123.9	123.3	124.1
Torsion angle (°)				
C5-N7-N12-C13	-178.5	175.7	179.1	176.2
N12-N7-C5-C6	178.9	179.1	-0.3	179
O8-C6-C5-N7	7	-4	0.5	-4.128
C1-C6-C5-N7	-172.9	177.8	-178.5	-177.7
O8-C6-C5-C4	-174.1	177.6	-178.3	-177.4
N7-C5-C4-O9	-3.2	5	6.7	4.823
C6-C5-C4-09	178	-176.7	-174.4	-176.8

N7-N12-C13-C14	169.6	142.184	-1.1	144
N7-N12-C13-C18	-10.8	.36.018	-179.81	-34
N12-C13-C18-C17	179.3	174.7	179.6	174.3
C23-O22-C16-C15	4.3	-0.866	-	-
C23-O22-C16-C17	-177.9	179.9	-	-
C18-C17-C16-O22	-177.8	179.1	-	-
O22-C16-C15-C14	177.4	178.7	-	-
C16-C17-C18-N19	180	-172.2	-179.9	-171.9
N12-C13-C14-C15	-179.5	-177	-179.63	-176.6
N12-C13-C18-N19	0.3	-10.5	-0.7	-10.9
C18-C13-C14-N19	-179.3	-7.7	-179.46	171.1
O21-N19-C18-C17	4.3	139.3	172.8	139.2
O20-N19-C18-C17	-174.5	-36.4	-7.8	-36.3
O21-N19-C18-C13	-175.4	-35.7	-6.9	-35.8
O20-N19-C18-C13	5.8	148.5	172.5	148.6

Table 4

COMPOUND	HOMO	LUMO	HOMO-1	LUMO+1
CD1	-6.3560	-2.9827	-2.9827	-6.5570
CD2	-6.5550	-6.6147	-2.9999	-6.6147

Table 5.

Mulliken atomic charges for CD1 & CD2			
CD1		CD2	
Atoms	Charges	Atoms	Charges
C1	-0.31357	C1	0.009795
C2	-0.00013	C2	0.012599
C3	-0.30641	C3	0.02642
C4	0.378326	C4	0.360598
C5	0.094371	C5	0.103409
C6	0.326406	C6	0.327362
C7	-0.16999	N7	-0.17065
C8	-0.40535	O8	-0.40108
C9	-0.51566	O9	-0.49546
C10	-0.41338	C10	0.028729
C11	-0.38687	C11	0.009606
N12	-0.54766	N12	-0.17042
C13	0.34339	C13	0.365218
C14	-0.14427	C14	0.011951
C15	-0.12544	C15	0.003507
C16	0.282039	C16	0.111672
C17	-0.12082	C17	0.029818
C18	0.331518	C18	0.325775
N19	0.067019	C19	0.067155
O20	-0.26836	O20	-0.27348
O21	-0.29831	O21	-0.28715
O22	-0.54322	C22	0.004613
C23	-0.18095		

Table 6

CD1		CD2		
Observed values	**DFT**	**Observed values**	**DFT**	**Approximate assignments**
3446	-		-	ν_{N-H}
3107	3144		3004	ν_{C-H} (aromatic)
2974	2925	2948	2920	N_{C-H} (aliphatic)
1739	1635	1685	1636	$\nu_{C=O}$
1639	1611	1642	1558	$\nu_{C=N}$
1537	1520	1568	1509	Assymetric stretching of NO_2 group
1342	1370	1343	1384	symmetric stretching of NO_2 group
976	999	975	914	ν_{N-O} stretching
857	874	852	878	ν_{C-N} stretching
755	741	758	768	aromatic C-H out of plane bending
672	618	627	617	aromatic C-C out of plane bending vibration

Table 7